αE-catenin is an autoinhibited molecule that coactivates vinculin

Hee-Jung Choi[a], Sabine Pokutta[a], Gregory W. Cadwell[b], Andrey A. Bobkov[b], Laurie A. Bankston[b], Robert C. Liddington[b], and William I. Weis[a,1]

[a]Departments of Structural Biology and Molecular and Cellular Physiology, Stanford University School of Medicine, 299 Campus Drive, Stanford, CA 94305; and [b]Program on Infectious Diseases, Sanford-Burnham Medical Research Institute, 10901 North Torrey Pines Road, La Jolla, CA 92037

Edited by Barry Honig, Columbia University/Howard Hughes Medical Institute, New York, NY, and approved April 6, 2012 (received for review March 6, 2012)

αE-catenin, an essential component of the adherens junction, interacts with the classical cadherin–β-catenin complex and with F-actin, but its precise role is unknown. αE-catenin also binds to the F-actin-binding protein vinculin, which also appears to be important in junction assembly. Vinculin and αE-catenin are homologs that contain a series of helical bundle domains, D1–D5. We mapped the vinculin-binding site to a sequence in D3a comprising the central two helices of a four-helix bundle. The crystal structure of this peptide motif bound to vinculin D1 shows that the two helices adopt a parallel, colinear arrangement suggesting that the αE-catenin D3a bundle must unfold in order to bind vinculin. We show that αE-catenin D3 binds strongly to vinculin, whereas larger fragments and full-length αE-catenin bind approximately 1,000-fold more weakly. Thus, intramolecular interactions within αE-catenin inhibit binding to vinculin. The actin-binding activity of vinculin is inhibited by an intramolecular interaction between the head (D1–D4) and the actin-binding D5 tail. In the absence of F-actin, there is no detectable binding of αE-catenin D3 to full-length vinculin; however, αE-catenin D3 promotes binding of vinculin to F-actin whereas full-length αE-catenin does not. These findings support the combinatorial or "coincidence" model of activation in which binding of high-affinity proteins to the vinculin head and tail is required to shift the conformational equilibrium of vinculin from a closed, autoinhibited state to an open, stable F-actin-binding state. The data also imply that αE-catenin must be activated in order to bind to vinculin.

Cadherin cell adhesion molecules mediate cell-cell adhesion. In the adherens junction, the cytoplasmic domain of classical cadherins binds to β-catenin that in turn binds to the F-actin-binding protein α-catenin. The cadherin–catenin complex thereby mediates a functional interaction with the actomyosin cytoskeleton (1, 2). The association of the actin cytoskeleton with cadherins is thought to be essential for the mechanical stability of solid tissues and for enabling cell and tissue shape changes during morphogenesis (3–9).

The role of α-catenin in cadherin-containing junctions has not been defined precisely. Although it might serve as a linker that directly connects the cadherin–β-catenin complex to filamentous actin, biochemical reconstitution with purified proteins indicated that binding of the cadherin–β-catenin complex to αE(epithelial)-catenin reduces binding of αE-catenin to F-actin (10, 11). Thus, it is not clear whether αE-catenin alone can serve as a physical link between the cadherin–catenin complex and F-actin. Several F-actin-binding proteins have been shown to bind to α-catenin and to localize to cell–cell contacts including l-afadin (12, 13), ZO-1 (14, 15), EPLIN (16), and vinculin (17, 18). The roles of these proteins in cell–cell junctions are poorly understood, but they might provide additional linkages to F-actin, perhaps in a manner specific to certain cell types or when the contacts are under particular mechanical loads.

Sequence alignments and structural data reveal that α-catenin and vinculin contain homologous segments (Fig. 1*A*). The crystal structure of full-length vinculin shows that it is composed of a series of helical bundles that form five distinct domains, designated D1-5 (19, 20) (Fig. 1*A*). D1, D2, and D3 each comprise two four-helix bundles that share a central, long helix. The two four-helix substructures of these domains are denoted "a" and "b" (Fig. 1*A*). D4 is a single four-helix bundle, and D5 is a single five-helix bundle (19, 20). In αE-catenin, D1 includes the β-catenin-binding and homodimerization sites and is structurally similar to vinculin D1 (19–22). D2 is absent in α-catenin, and this is the most significant difference between these two proteins. The D3a sequence of αE-catenin has not been structurally characterized, whereas the αE-catenin D3b and D4 helical bundles correspond to the proteolytically and structurally defined middle or "M" domain (Fig. 1*A*) that binds l-afadin (12, 23). The C-terminal actin-binding D5 of vinculin and α-catenin is the region of highest homology; however, α-catenin bears an extra C-terminal extension that is also required for actin binding (12). α-Catenin has a similar length linker between D4 and D5 but lacks the proline-rich motif that mediates vinculin interactions with vinexin and other proteins (19).

Vinculin has been best characterized as a component of focal adhesions, where it appears to modulate adhesiveness in response to force (24–26). Vinculin in isolation does not bind to F-actin as it adopts an autoinhibited, closed conformation in which the actin-binding domain D5 (the "tail") forms extensive interactions with the D1–D4 "head". Activation of actin binding by vinculin requires interaction with additional proteins such as talin (and possibly α-actinin), which bind to the head region and/or interactions with the proline-rich region that links the head and tail (19, 27–30)

Unlike vinculin, αE-catenin binds F-actin constitutively. This may be due to the lack of the D2 region that, in vinculin, forms a stabilizing bridge that locks the D1 and D3 domains into positions that promote the autoinhibitory interaction with D5 (19, 20). Nonetheless, several observations suggest that many ligand-binding activities of αE-catenin are regulated because it adopts distinct conformations in the presence of different binding partners. First, αE-catenin forms homodimers. The homodimerization and β-catenin binding sites overlap such that αE-catenin is a monomer when bound to the cadherin–β-catenin complex. Limited proteolysis of αE-catenin monomer, homodimer, and a chimera that mimics the heterodimer with β-catenin revealed distinct digestion patterns suggestive of conformational differences (10). Second, αE-catenin D4 acts as an "adhesion modulation domain" because deletion of this domain weakens cell-cell adhesion (15). Vinculin binds to the D3 region of αE-catenin (15, 19). Vinculin is recruited to cell-cell contacts in a myosin II

Author contributions: H.-J.C., S.P., L.A.B., R.C.L., and W.I.W. designed research; H.-J.C., S.P., G.W.C., and A.A.B. performed research; H.-J.C., S.P., L.A.B., R.C.L., and W.I.W. analyzed data; and R.C.L. and W.I.W. wrote the paper.

The authors declare no conflict of interest.

This article is a PNAS Direct Submission.

Data deposition: Coordinates and structure factors have been deposited in the Protein Data Bank, www.pdb.org (PDB ID codes 4E18 and 4E17).

[1]To whom correspondence should be addressed. E-mail: bill.weis@stanford.edu.

This article contains supporting information online at www.pnas.org/lookup/suppl/doi:10.1073/pnas.1203906109/-/DCSupplemental.

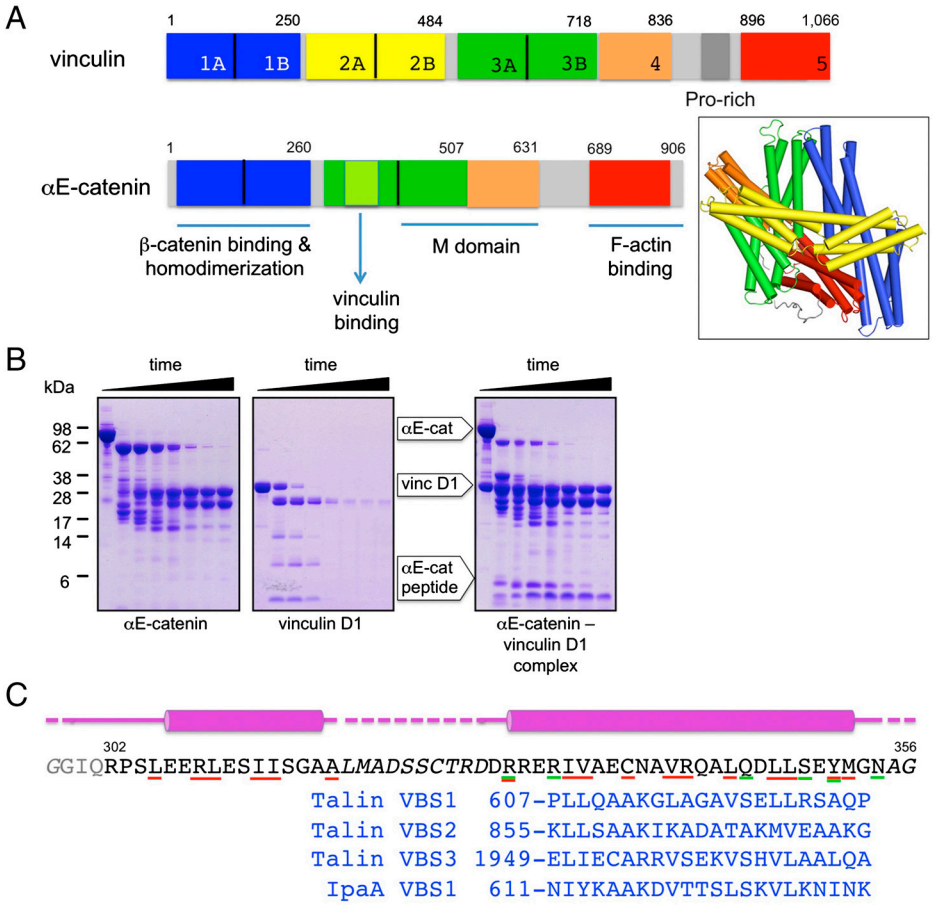

Fig. 1. (*A*) Primary structures of αE-catenin and vinculin with domains observed in the vinculin crystal structure (*Inset*) and several functional binding sites indicated. (*B*) Trypsin digestion of full-length αE-catenin dimer, vinculin D1 and the full-length αE-catenin–vinculin D1 complex. The region of αE-catenin protected by D1 in the complex is indicated. (*C*) Sequence of αE-catenin protected from trypsin by vinculin D1. Residues shown in gray originate from the expression vector and remain after cleavage of the N-terminal GST affinity tag. Hydrophobic residues that interact with vinculin are underlined in red, and residues that form polar contacts are underlined in green. Italicized residues are not visible in the structure.

force-dependent manner (31–33), and the D4 region of αE-catenin inhibits vinculin recruitment to cell–cell contacts in the absence of myosin-dependent force, implying that a force-induced conformational change in αE-catenin is required for vinculin binding (33).

Here, we define the vinculin-binding site of αE-catenin by biochemical and structural methods as the second and third helices of the D3a bundle, one of which is activation independent. Isothermal titration calorimetry (ITC) measurements reveal that the recombinant D3 region of αE-catenin mediates strong binding to vinculin constructs lacking the tail domain, whereas longer constructs containing either or both of the first α-helix of D1a and D4 of α-catenin significantly weaken vinculin binding. Finally, we show that only the stronger-binding fragment of αE-catenin is able to prime vinculin for binding to actin, consistent with the notion that overcoming the strong autoinhibitory intramolecular head–tail interaction requires input from more than one binding event (19, 34). Our data also imply that αE-catenin itself requires activation in order to contribute to vinculin activation.

Results

Defining the Vinculin-Binding Site of αE-Catenin. The binding site for vinculin on αE-catenin was originally mapped by deletion mutagenesis to a region of αE-catenin spanning residues 327–402 (15). In that study, vinculin recruitment to cell–cell contacts was monitored after transfection of E-cadherin/αE-catenin fusion proteins. To map the interaction in further detail with purified proteins, we produced recombinant αE-catenin D3, residues 273–510 (Fig. 1*A*).

ITC analysis showed that αE-catenin D3 bound with high affinity to vinculin constructs lacking the tail (D5) but did not bind detectably to full-length vinculin (Tables 1 and 2), consistent with the notion that αE-catenin binds only to activated vinculin. In this sense, its behavior is similar to all other known ligands to the vinculin head with the possible exception of the invasin IpaA from the pathogen *Shigella flexneri* (35). Similar affinities were observed using isolated vinculin D1 or the larger vinculin head construct D1–D4 (5–15 nM), similar to the result previously obtained for D1–D3 (19, 36) (Table 1 and Figs. S1 and S2), confirming that vinculin D1 contains the full binding site for αE-catenin. In the closed conformation of vinculin, interactions with the tail domain lock D1 into a conformation that does not bind ligands (19), explaining the lack of αE-catenin D3 binding to the full-length, inactive vinculin.

The purified complex of full-length αE-catenin dimer and vinculin D1 was digested with trypsin in order to define the physical boundaries of the vinculin-binding site on αE-catenin (Fig. 1*B*). An approximately 6 kDa fragment was protected, and N-terminal sequencing and mass spectrometry revealed that it spans residues 301–357. This sequence corresponds to the second and third helices of the vinculin-like D3a domain. Interestingly, the vinculin-binding site mapped by deletion mutagenesis comprises only the third helix of D3a (15), which contains the consensus vinculin-binding motif (37); however, the region between helices 2 and 3 contains a basic residue that would likely be cleaved by trypsin in solution (Fig. 1*D*), suggesting that the proteolytically defined fragment is protected by vinculin. Unfortunately, we were unable to measure the affinity of this fragment for vinculin D1, as it could not be produced in isolation without significant degradation.

Structure of the αE-Catenin–Vinculin Complex. To visualize directly the αE-catenin–vinculin interaction, αE-catenin residues 302–356 were expressed in *Escherichia coli* as a C-terminal fusion to GST. Lysates from these cells were mixed with lysates of cells expressing vinculin D1, and the complex purified after removal of the GST tag. A similar strategy was used to purify the complex of vinculin D1 with a shorter αE-catenin fragment, residues

Table 1. ITC data for αE-catenin constructs binding to vinculin D1 or D1–D4

αE-catenin variant/complex	Vinculin variant	K_D (M)	ΔH (kcal/mol)	TΔS (kcal/mol)	ΔG (kcal/mol)
αE-cat full dimer	+ D1	$1.1(\pm0.2)\times10^{-6}$	13.8 ± 0.2	21.9	−8.1
	+ D1–D4	$2.4(\pm0.4)\times10^{-6}$	5.2 ± 0.2	12.9	−7.7
αE-cat full monomer	+ D1	$1.8(\pm0.2)\times10^{-6}$	12.6 ± 0.6	20.4	−7.8
αE-cat full+/βcat+/E-cadherin cytoplasmic domain ternary complex	+ D1	$1.9(\pm0.4)\times10^{-6}$	1.4 ± 0.1	9.2	−7.8
$\alpha E\text{-cat}^{1-651}$ (dimer)	+ D1	$1.3(\pm0.1)\times10^{-6}$	12.8 ± 0.2	20.9	−8.1
	+ D1–D4	$2.7(\pm0.3)\times10^{-6}$	10.4 ± 0.4	18.0	−7.6
$\alpha E\text{-cat}^{1-510}$ (dimer)	+ D1	$0.2(\pm0.1)\times10^{-6}$	6.2 ± 0.2	15.3	−9.1
αE D3 (monomer)	+ D1	$5.2(\pm0.3)\times10^{-9}$	9.9 ± 0.1	21.2	−11.3
	+ D1–D4	$15(\pm1.5)\times10^{-9}$	11.1 ± 0.1	21.7	−10.6
$\alpha E^{273-651}$ (monomer)	+ D1	$2.0(\pm0.2)\times10^{-6}$	10.4 ± 0.2	18.2	−7.8
αEcat-βcat chimera	+ D1	$0.21(\pm0.02)\times10^{-6}$	18.0 ± 0.1	27.1	−9.1
αE^{57-906} (dimer)	+D1	$36(\pm0.5)\times10^{-9}$	5.8 ± 0.1	15.9	−10.1

321–356 that corresponds to the third helix of D3a bearing the consensus vinculin D1 binding motif (37). The purified complexes were crystallized and their three-dimensional structures determined (Fig. 2 and Table S1). The crystals diffracted to similar resolutions, and the common portion of the structures show no significant differences, so the description here refers to the longer complex. Residues 302–317 and 328–354 are visible in the structure. Residues 304–316 form a α helix that binds to the C-terminal bundle of vinculin D1 (D1b), and a helix spanning 328–353 binds to the N-terminal bundle (D1a). The two helices are roughly colinear and separated by approximately 18 Å, a distance that can be readily spanned by the intervening nine residues.

The αE-catenin helix 328–353 inserts between the first and second helices of vinculin D1a, which separate and straighten to accommodate the new helix into a five-helix bundle. All five helices contribute to a single hydrophobic core of the bundle, a process that has been termed "bundle conversion" (21) (Fig. 2). Although the two helices are exposed on the surface of full-length vinculin, the reorganized bundle can no longer bind the vinculin tail. In particular, vinculin helix 1 changes its disposition sufficiently that it can no longer support tail binding; i.e., the low affinity of full-length vinculin for head ligands arises from allosteric constraints on the four-helix bundle present in the autoinhibited conformation. A similar reorganization has been observed in a number of vinculin D1 complexes with "vinculin-binding site" (VBS) peptides derived from endogenous [e.g., talin (21, 37) and α-actinin (38)] and pathogenic [e.g., *Shigella flexneri* IpaA (35, 39) and *Rickettsia* surface cell antigen 4 (40)] proteins. With the exception of α-actinin, whose helix binds in the reverse orientation, the complexes are closely superimposable, with rmsds <1 Å.

In contrast to the binding of the αE-catenin 328–353 helix, the interaction of the αE-catenin 304–316 helix with vinculin is unique. This helix is also amphipathic, and inserts a hydrophobic ridge comprising Ile and Leu residues into a groove between the first and second helices at the distal end of the D1b bundle. In this case, however, the helix attaches to the side of the 4-helix bundle rather than inserting into it, leaving the hydrophobic core of the 4-helix bundle intact (Fig. 2). Moreover, the binding site is fully exposed in the auto-inhibited conformation of vinculin suggesting that binding at this subsite is activation-independent. The relative contribution of this helix to the overall binding interaction cannot be assessed quantitatively as we have not been able to purify the cocrystallized αE-catenin peptides to homogeneity; however, we note that the 328–354 helix buries a much larger surface area than 304–316 (1,240 $Å^2$ vs. 424 $Å^2$), suggesting that it is the principal determinant of the αE-catenin-vinculin interaction. The virulence factor (IpaA), which is a mimetic of talin and αE-catenin, also utilizes a second helix that binds D1b bundle

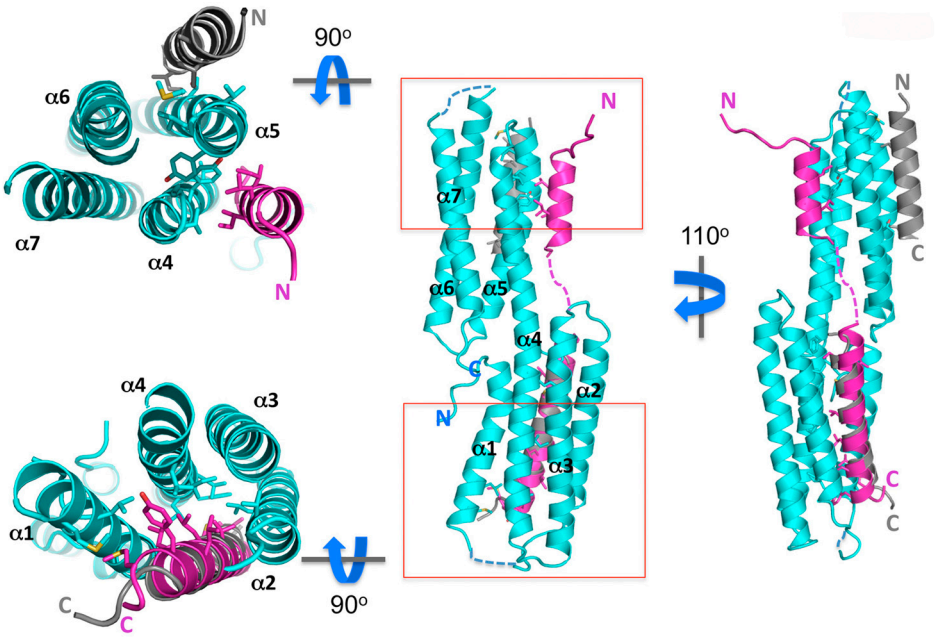

Fig. 2. Crystal structure of $\alpha E\text{-catenin}^{302-356}$ bound to vinculin D1. αE-catenin is shown in magenta and vinculin in turquoise. Also shown in gray is the bound Shigella IpaA peptide. Interacting hydrophobic side chains are shown in stick representation.

of vinculin and does not induce rearrangement (39). In this case, however, the helix binds to an exposed groove formed by helices 2 and 3 rather than 1 and 2 (Fig. 2).

Sequence alignment of αE-catenin and vinculin suggests that the two vinculin-binding αE-catenin helices are organized as adjacent, antiparallel helices in the D3a four-helix bundle. Although no structural data are available, three further lines of evidence suggest that this bundle is indeed present in αE-catenin and that it disassembles upon binding vinculin. First, the circular dichroism spectra of αE-catenin D3 in isolation or bound to vinculin D1 are very similar (Fig. S3) indicating that αE-catenin D3 has similar helical content when free or bound to vinculin. Second, the high-affinity interaction with vinculin D1 is endothermic and entropy-driven (Table 1 and Fig. S1), consistent with an unfolding process. Third, gel filtration and multiangle light scattering indicate that αE-catenin D3 and vinculin D1 form a complex with a 2:2 stoichiometry (Fig. S4). This is likely due to dimerization and stabilization of one or both of the D3a helices that are left unpaired upon exposure of the vinculin-binding helices, given that there is no net loss of helical content upon complex formation and that both of the crystallized complexes, which lack the first and fourth helices of D3a, size as monomers during the gel filtration step of purification.

Modulation of Vinculin-Binding Affinity by Other Regions of αE-Catenin. The "adhesion modulation domain" that corresponds to αE-catenin D4 appears to mask the vinculin-binding site in the absence of force (15, 33). We used ITC to measure quantitatively the effect of various portions of αE-catenin on the high-affinity binding to vinculin displayed by D3. αE-catenin$^{273–651}$, which includes D3 and D4, shows markedly weaker binding to vinculin than D3, with K_Ds in the low μM range for vinculin D1 and vinculin D1–D4 (Table 1 and Figs. S1 and S2). K_D values in the single μM range were also observed for the full-length αE-catenin dimer and monomer as well as the ternary complex of E-cadherin cytoplasmic domain, full-length β-catenin, and full-length αE-catenin (Table 1 and Fig. S1).

A chimera comprising a minimal α-catenin-binding fragment of β-catenin (residues 118–151) fused to residues 55–906 of αE-catenin mimics the interaction of these two proteins (11, 22). The chimera binds to vinculin D1 approximately 10x more strongly than full-length αE-catenin or the ternary complex of E-cadherin, β-catenin and αE-catenin (Table 1 and Fig. S1). Crystal structures have shown that residues 118–151 of β-catenin combine with a helix encompassing αE-catenin residues 57–80 to form a four-helix bundle with helices 2–4 of αE-catenin D1a (22). In the absence of β-catenin, residues 57–80 are flexibly linked to the rest of the protein, as indicated by proteolytic sensitivity (22). Surprisingly, isolated αE-catenin$^{57–906}$ bound to vinculin D1 more strongly than the chimera, with a K_D of 36 nM. These data suggest that the N-terminal 56 residues of αE-catenin contribute to the weakened affinity for vinculin relative to αE-catenin D3.

In order to bind to vinculin, the second and third helices of αE-catenin D3a must dissociate from the four-helix bundle and adopt a parallel, almost colinear arrangement (Fig. 2). Modeling suggests that the long linker between D1 and D3, the long loop between the first and second helix of D3a, and the irregular kink between the last helix of D3a and D3b provide sufficient flexibility to enable this transition (Fig. 3). In our models, D4 and D1a lie near the vinculin-bound helices (Fig. 3). The proximity of these regions provides a rationale for why removing the D4 or the N-terminal 56 residues increases the affinity of αE-catenin for vinculin (Table 1): These regions would restrict, sterically or allosterically, the conformational space available for achieving the opening of the four-helix bundle needed to expose the vinculin-binding helices. Of course, the models in Fig. 3 are necessarily speculative in the absence of a full-length αE-catenin structure, and we cannot rule out alternatives such as conformational effects on D3a caused by deletion of various regions of αE-catenin.

Relationship of Binding Affinity and Activation of Vinculin

No single ligand has been demonstrated to significantly disrupt the head-tail interaction in full-length wild-type vinculin. In the case of talin, coincubation with the tail ligand F-actin is sufficient to activate vinculin (34) presumably because the binding of head and tail ligands are structurally and energetically coupled (19). In order to demonstrate this linkage in the case of αE-catenin binding to vinculin, we engineered full-length vinculin to have weakened or enhanced head-tail association, and measured binding to αE-catenin D3 by ITC. We compared wild-type vinculin with the following mutants: (*i*) VM1, a Cys-Ser mutant at position 85 that is surface-exposed on the third helix of D1a and does not directly contact αE-catenin, and (*ii*) two additional mutants in the C85S background: VM2, a double mutation (N773A/E775A) in vinculin D4 (at the D4-D5 interface) that was previously shown to subtly weaken head–tail interactions, (41); and (*iii*) VM3, the mutant A50I that we previously engineered to stabilize D1 as well as the head-tail interaction, thereby inhibiting the conformational changes required for helical insertion by head ligands (19).

As predicted, wild-type vinculin shows no measurable binding to αE-catenin D3 (Table 2 and Fig. S5); however, the C85S mutation in D1 led to a weak but measurable affinity for the αE-catenin fragment with a $K_D \sim 12$ μM. The second mutation, at the D4–D5 interface, had an additive effect leading to a K_D of 160 nM that was close to that of binding to the free vinculin head. In contrast, the A50I mutation returned binding to an undetectable (wild-type) level, indicating that it was dominant over the weakening effect of the C85A mutation. These results emphasize

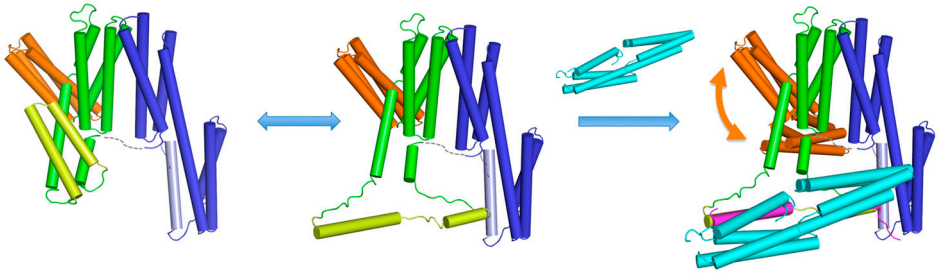

Fig. 3. Model of vinculin D1 (cyan) binding to αE-catenin. (*Left*) Model of αE-catenin based on the vinculin crystal structure. The D2 domain was deleted and the flexibility between D3b and D4 in crystal structures of the αE-catenin M domain (12, 23) was modeled by superimposing the D3b bundles of vinculin and αE-catenin and considering the range of positions adopted by αE-catenin D4. For clarity, the actin-binding domain D5 has been omitted from the figure because it has no effect on the affinity for vinculin and is likely flexibly linked to the rest of the protein. (*Middle*) The two vinculin-binding helices (light green) have been modeled as observed in the crystal structure bound to vinculin D1 with physically plausible connections made to D1 and to D3b. (*Right*) The structure of the complex between vinculin D1 (cyan) and αE-catenin$^{302–356}$ (magenta) has been superimposed on the speculative "open" αE-catenin model. Domains are colored as in Fig. 1, and the D3a helices that bind to vinculin are colored as in Fig. 2.

Table 2. ITC data for full-length vinculin constructs binding to αE-catenin D3

Protein	K_D (M)	ΔH (kcal/mol)	TΔS (kcal/mol)	ΔG (kcal/mol)
Vinculin w.t.	ND	—	—	—
Vinculin VM1	12×10^{-6}	−8.6	−1.9	−6.7
Vinculin VM2	0.19×10^{-6}	−12.5	−3.4	−9.1
Vinculin VM3	ND	—	—	—

ND = No Detectable binding.
VM1 = point mutation C85S + Cys-Gly insertion between residues 344–345.
VM2 = VM1 + N773A/E775A
VM3 = VM1 + A50I.
The double mutant N773A/E775A was described in ref. 41.
The A50I mutant was described in ref. 19.

how important it is to use either wild-type vinculin or fully characterized variants in order to evaluate properly the biological roles of its ligands.

Next, we tested the ability of αE-catenin D3 to coactivate vinculin in an actin cosedimentation assay that qualitatively detects coupling of head-binding ligands with tail binding to F-actin. We observed significant cosedimentation at concentrations >5 μM αE-catenin D3 (Fig. 4). In contrast, the longer fragment, αE-catenin$^{1–651}$, which lacks only the actin-binding domain, did not promote actin binding up to the highest concentrations tested (40 μM). Full-length αE-catenin in any of its oligomeric forms (monomer, homodimer, or as part of the E-cadherin–β-catenin complex) binds to the vinculin head with the same (low) affinity as αE-catenin$^{1–651}$ (Table 1). Thus, the ability of αE-catenin fragments to coactivate vinculin correlates with their affinity for the isolated vinculin head, consistent with the model of thermodynamic coupling.

Discussion

Vinculin requires coactivation by focal adhesion proteins such as talin, which binds D1, and/or interactions with the proline-rich region that links the head and tail, in order to stimulate actin binding (19, 28, 29). A recent report (36), as well as the data presented here, demonstrate that the adherens junction protein αE-catenin can also contribute to vinculin activation. Vinculin activation is best understood in terms of an open-closed equilibrium that lies strongly toward the closed state in the absence of binding partners (the estimated head–tail K_D is ≤nM for the full-length protein) (19). The small fraction of free head and tail present at equilibrium can bind to other proteins (e.g., F-actin to the D5 tail), and these interactions pull the equilibrium

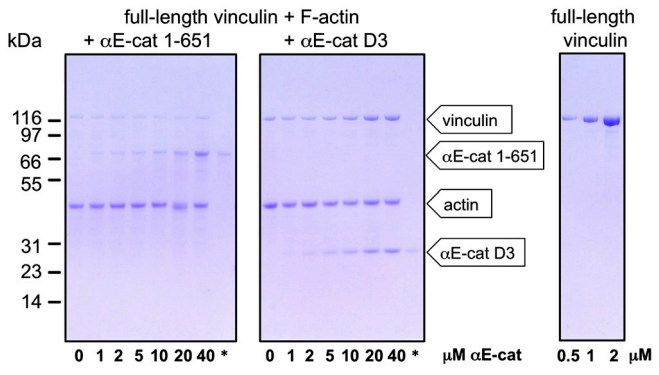

Fig. 4. Vinculin activation assays. Pelleting of 10 μM full-length vinculin with F-actin is shown as a function of increasing concentrations of αE-catenin D1–D4 (*Left*) or αE-catenin D3 (*Middle*). The lanes marked asterisk (*) show the background sedimentation of the αE-catenin fragment at 10 μM in the absence of F-actin. For comparison, the gel on the right shows the equivalent amount of vinculin loaded at the indicated concentrations.

towards the open state; however, we know of no single binding partner that provides sufficient energy to stabilize a significant population of open, active vinculin. In this context, it should be noted that isolated head and tail components of vinculin form a much weaker head–tail complex with $K_D \leq$ μM) that can be readily separated by active fragments of their ligands (42).

A protein that binds tightly to the vinculin head will be able to form stable complexes with the small fraction of "exposed" head present in the equilibrium population of full-length vinculin more readily than a weakly binding partner. This is seen for αE-catenin D3 relative to, for example, full-length αE-catenin (Table 1). Because binding to F-actin also favors the open conformation of vinculin, the effective affinity of a partner for the vinculin head is greater in the presence of F-actin than in its absence. This explains why no binding of αE-catenin D3 to full-length vinculin is seen at 90 μM (Table 2), whereas detectable activation occurs above 5 μM (Fig. 4). Similar results were reported using a modified vinculin in which fluorescent proteins are inserted between the head and tail and at the C terminus that reports on the opening of vinculin (36).

Peng et al. suggested that α-catenin uses a novel mechanism to activate vinculin (36)—i.e., distinct from the way talin activates vinculin at focal adhesions. This proposal was based in large part on the ability of αE-catenin, but not talin, to coactivate the A50I mutant of vinculin; however, our structural data indicate that the underlying mechanism of helix insertion into the vinculin D1a bundle by helix 3 of αE-catenin D3a is analogous to that of talin. On the other hand, the structure revealed an additional interaction with helix 2 that interacts with a constitutively exposed binding site on vinculin D1b. One possibility is a two-step interaction, in which αE-catenin weakly and transiently occupies the D1b site in auto-inhibited vinculin (we do not detect binding of αE-catenin D3 to auto-inhibited vinculin). If a tail ligand such as F-actin is encountered while this site is occupied, then a rapid activation-dependent insertion of the second helix may ensue owing to the high local concentration of αE-catenin, which could be kinetically captured in the cosedimenation assay. Note that under equilibrium solution conditions, αE-catenin does not interact with the A50I mutant (Table 2).

The weak binding of αE-catenin$^{1–651}$ to the vinculin head (Table 1) is consistent with its inability to activate vinculin (Fig. 4). Because the affinity of this fragment for vinculin is the same as those of full-length αE-catenin, either free or bound to the cadherin–β-catenin complex, it is likely that αE-catenin cannot activate vinculin by itself. No binding of αE-catenin to full-length vinculin is observed in ITC at a concentration of 90 μM, which sets a lower limit on the affinity of this interaction at a K_D of 9 mM (assuming detection of the 1% bound at 100x K_D). We cannot rule out that αE-catenin can bind to a significant number of vinculin molecules if the concentrations of these proteins at cell–cell contacts is sufficiently high, but the effective concentrations at these contacts are not known.

A cytosolic pool of inactive vinculin is recruited to nascent focal adhesions, where it strengthens cell-extracellular matrix adhesion in a force-dependent manner. It appears that this inactive pool of vinculin can also be recruited to cell–cell contacts in a force-dependent manner (32, 33). The data presented here strongly suggest that full-length αE-catenin binds to vinculin too weakly to effect activation. Thus, it is very likely that αE-catenin itself must be activated in order to make its vinculin-binding site sufficiently accessible to enable high-affinity binding to the vinculin head region. The nature of this activation is unclear at present, but possibilities include binding of other proteins such as l-afadin (12, 13), ZO-1 (14, 15), and EPLIN (16), posttranslational modification, and/or mechanical force (33).

Materials and Methods

Protein Constructs and Purification. Mouse αE-catenin and chicken vinculin were used for all experiments. All proteins were expressed in *E. coli* and purified as described in *SI Text*. The chimeric β-catenin–αE-catenin protein, full-length β-catenin, and the cytoplasmic domain of E-cadherin were expressed and purified as previously described (11, 43).

For crystallization, two different constructs of vinculin D1 binding region of αE-catenin, αE-catenin$^{302–356}$ and αE-catenin$^{321–356}$ were designed based on limited proteolysis or secondary structure prediction and homology modeling, respectively. Each was expressed as GST fusion protein. After induction, the pelleted cells were resuspended and mixed with the harvested cells expressing GST-vinculin D1. The mixture of cell suspensions was lysed and the complexes purified directly using glutathione agarose affinity chromatography, TEV protease cleavage, ion exchange chromatography, and gel filtration (see *SI Text*).

Isothermal Titration Calorimetry. ITC experiments summarized in Table 1 were performed on a VP-ITC calorimeter (Microcal, GE Healthcare). A total of 30–40 7 μl aliquots of 100–700 μM vinculin D1 or head domain was injected into the cell, which contained 10–50 μM αE-catenin at 25 °C. For each experiment, a control run in which the same concentration of vinculin protein solution was injected into H1 buffer was used for baseline subtraction. Experiments with wild-type and mutant full-length vinculins and vinculin D1-D3 (Table 2) were performed on an ITC200 calorimeter (Microcal) at 23 °C in 20 mM Hepes, pH 7.4, 150 mM NaCl, and 1 mM β-mercaptoethanol. A total of 19 2.0 μl aliquots of 1.3 mM αE-catenin D3 (residues 273–510) were injected into the cell that contained 90 μM vinculin. Data were analyzed with Microcal Origin software.

Limited Proteolysis. For limited proteolysis experiments 12 μM full-length αE-catenin dimer, vinculin D1 (residues 1–258), and purified αE-catenin dimer–vinculin D1 complex were incubated at room temperature with 14 μg/mL sequencing grade trypsin (Roche). Reactions were stopped after 5′, 15′, 30′, 1 h, 2 h, 3 h, and 4 h by boiling for 5 min in SDS gel loading buffer. The reactions were analyzed by SDS/PAGE. An approximately 6 kDa band stabilized only in the αE-catenin dimer–vinculin D1 complex was cut out and analyzed by mass mapping. For N-terminal sequencing, the gel was electroblotted onto a PVDF membrane and the approximately 6 kDa band excised.

Crystallographic Procedures. Crystals of the αE-catenin$^{321–356}$–vinculin D1 complex were obtained vapor diffusion against a reservoir solution consisting of 20% PEG8000, 100 mM MES (pH 6.8), and 3 mM DTT at 10 °C. The αE-catenin$^{302–356}$–vinculin D1 complex was crystallized at 20 °C with a reservoir solution containing 22% PEG3350, 100 mM bis-Tris-propane (pH 8.0), 100 mM sodium nitrate, and 3 mM DTT. Diffraction data were measured on beamline 23-ID-D at the Advanced Photon Source, and the structures solved by molecular replacement. Detailed procedures, data collection, and model refinement statistics are provided in the *SI Text*.

Actin-Binding Assay. Chicken skeletal muscle actin was polymerized overnight by adding actin polymerization buffer to a final concentration of 20 mM imidazole, pH 7.0, 100 mM KCl, 2 mM $MgCl_2$, 0.5 mM ATP, and 1 mM EDTA. F-actin at 2 μM was incubated for 30 min at room temperature with 10 μM full-length vinculin and increasing amounts of αE-catenin D3 or αE-catenin$^{1–651}$. The buffer used for dilutions was 20 mM Hepes pH 8.0, 150 mM NaCl, 2 mM $MgCl_2$, 0.5 mM ATP, 1 mM EGTA, and 1 mM DTT. Unbound and actin-bound protein was separated by centrifugation for 10 min at 100,000 rpm in a Beckman TLA 120.1 rotor. After removal of the supernatant, pellets were resuspended in gel loading buffer and analyzed by SDS/PAGE.

ACKNOWLEDGMENTS. We thank Sandro Vivona for assistance with multiangle light scattering analysis, and Adam Kwiatkowski and James Nelson for comments on the manuscript. Use of the Advanced Photon Source was supported by the US Department of Energy Contract no. DE-AC-02-06CH11357. This work was supported by National Institutes of Health Grants R01 GM56169 (to W.I.W.) and U01 GM09463 (to R.C.L. and W.I.W.).

1. Pokutta S, Weis WI (2007) Structure and mechanism of cadherins and catenins in cell-cell contacts. *Annu Rev Cell Dev Biol* 23:237–261.
2. Shapiro L, Weis WI (2009) Structure and biochemistry of cadherins and catenins. *Cold Spring Harb Perspect Biol* 1:a003053.
3. Dawes-Hoang RE, et al. (2005) Folded gastrulation, cell shape change and the control of myosin localization. *Development* 132:4165–4178.
4. Farge E (2011) Mechanotransduction in development. *Curr Top Dev Biol* 95:243–265.
5. Liu Z, et al. (2010) Mechanical tugging force regulates the size of cell-cell junctions. *Proc Natl Acad Sci USA* 107:9944–9949.
6. Tambe DT, et al. (2011) Collective cell guidance by cooperative intercellular forces. *Nat Mater* 10:469–475.
7. Martin AC, Kaschube M, Wieschaus EF (2009) Pulsed contractions of an actin-myosin network drive apical constriction. *Nature* 457:495–499.
8. Bertet C, Sulak L, Lecuit T (2004) Myosin-dependent junction remodeling controls planar cell intercalation and axis elongation. *Nature* 429:667–671.
9. Yonemura S (2011) A mechanism of mechanotransduction at the cell-cell interface: Emergence of α-catenin as the center of a force-balancing mechanism for morphogenesis in multicellular organisms. *Bioessays* 33:732–736.
10. Drees F, Pokutta S, Yamada S, Nelson WJ, Weis WI (2005) α-Catenin is a molecular switch that binds E-cadherin/β-catenin and regulates actin filament assembly. *Cell* 123:903–915.
11. Yamada S, Pokutta S, Drees F, Weis WI, Nelson WJ (2005) Deconstructing the cadherin-catenin-actin complex. *Cell* 123:889–901.
12. Pokutta S, Drees F, Takai Y, Nelson WJ, Weis WI (2002) Biochemical and structural definition of the l-afadin- and actin-binding sites of α-catenin. *J Biol Chem* 277:18868–18874.
13. Tachibana K, et al. (2000) Two cell adhesion molecules, nectin and cadherin, interact through their cytoplasmic domain-associated proteins. *J Cell Biol* 150:1161–1175.
14. Itoh M, Nagafuchi A, Moroi S, Tsukita S (1997) Involvement of ZO-1 in cadherin-based cell adhesion through its direct binding to a catenin and actin filaments. *J Cell Biol* 138:181–192.
15. Imamura Y, Itoh M, Maeno Y, Tsukita S, Nagafuchi A (1999) Functional domains of α-catenin required for the strong state of cadherin-based cell adhesion. *J Cell Biol* 144:1311–1322.
16. Abe K, Takeichi M (2008) EPLIN mediates linkage of the cadherin-catenin complex to F-actin and stabilizes the circumferential actin belt. *Proc Natl Acad Sci USA* 105:13–19.
17. Hazan RB, Kang L, Roe S, Borgen PI, Rimm DL (1997) Vinculin is associated with the E-cadherin adhesion complex. *J Biol Chem* 272:32448–32453.
18. Weiss EE, Kroemker M, Rüdiger A-H, Jockusch BM, Rüdiger M (1998) Vinculin is part of the cadherin-catenin junctional complex: Complex formation between α-catenin and vinculin. *J Cell Biol* 141:755–764.
19. Bakolitsa C, et al. (2004) Structural basis for vinculin activation at sites of cell adhesion. *Nature* 430:583–586.
20. Borgon RA, Vornrhein C, Bricogne G, Bois PRJ, Izard T (2004) Crystal structure of human vinculin. *Structure* 12:1189–1197.
21. Izard T, et al. (2004) Vinculin activation by talin through helical bundle conversion. *Nature* 427:171–175.
22. Pokutta S, Weis WI (2000) Structure of the dimerization and β-catenin binding region of α-catenin. *Mol Cell* 5:533–543.
23. Yang J, Dokurno P, Tonks NK, Barford D (2001) Crystal structure of the M-fragment of α-catenin: Implications for modulation of cell adhesion. *EMBO J* 20:3645–3656.
24. Diez G, et al. (2009) Anchorage of vinculin to lipid membranes influences cell mechanical properties. *Biophys J* 97:3105–3112.
25. Goldmann WH, et al. (1998) Differences in elasticity of vinculin-deficient F9 cells measured by magnetometry and atomic force microscopy. *Exp Cell Res* 239:235–242.
26. Humphries JD, et al. (2007) Vinculin controls focal adhesion formation by direct interactions with talin and actin. *J Cell Biol* 179:1043–1057.
27. Critchley DR, et al. (1999) Integrin-mediated cell adhesion: The cytoskeletal connection. *Biochem Soc Symp* 65:79–99.
28. Huttelmaier S, et al. (1998) The interaction of the cell-contact proteins VASP and vinculin is regulated by phosphatidylinositol-4,5-bisphosphate. *Curr Biol* 8:479–488.
29. Chen H, Choudhury DM, Craig SW (2006) Coincidence of actin filaments and talin is required to activate vinculin. *J Biol Chem* 281:40389–40398.
30. Kelly DF, et al. (2006) Structure of the α-actinin-vinculin head domain complex determined by cryo-electron microscopy. *J Mol Biol* 357:562–573.
31. Miyake Y, et al. (2006) Actomyosin tension is required for correct recruitment of adherens junction components and zonula occludens formation. *Exp Cell Res* 312:1637–1650.
32. le Duc Q, et al. (2010) Vinculin potentiates E-cadherin mechanosensing and is recruited to actin-anchored sites within adherens junctions in a myosin II-dependent manner. *J Cell Biol* 189:1107–1115.
33. Yonemura S, Wada Y, Watanabe T, Nagafuchi A, Shibata M (2010) α-Catenin as a tension transducer that induces adherens junction development. *Nat Cell Biol* 12:533–542.
34. Chen H, Choudhury DM, Craig SW (2006) Coincidence of actin filaments and talin is required to activate vinculin. *J Biol Chem* 281:40389–40398.
35. Hamiaux C, van Eerde A, Parsot C, Broos J, Dijkstra BW (2006) Structural mimicry for vinculin activation by IpaA, a virulence factor of *Shigella flexneri*. *EMBO Rep* 7:794–799.
36. Peng X, Maiers JL, Choudhury D, Craig SW, Demali KA (2012) α-Catenin uses a novel mechanism to activate vinculin. *J Biol Chem* 287:7728–7737.
37. Gingras AR, et al. (2005) Mapping and consensus sequence identification for multiple vinculin binding sites within the talin rod. *J Biol Chem* 280:37217–37224.
38. Bois PR, Borgon RA, Vonrhein C, Izard T (2005) Structural dynamics of α-actinin-vinculin interactions. *Mol Cell Biol* 25:6112–6122.
39. Nhieu GT, Izard T (2007) Vinculin binding in its closed conformation by a helix addition mechanism. *EMBO J* 26:4588–4596.
40. Park H, Lee JH, Gouin E, Cossart P, Izard T (2011) The rickettsia surface cell antigen 4 applies mimicry to bind to and activate vinculin. *J Biol Chem* 286:35096–35103.
41. Cohen DM, Chen H, Johnson RP, Choudhury B, Craig SW (2005) Two distinct head-tail interfaces cooperate to suppress activation of vinculin by talin. *J Biol Chem* 280:17109–17117.
42. Bois PR, O'Hara BP, Nietlispach D, Kirkpatrick J, Izard T (2006) The vinculin binding sites of talin and α-actinin are sufficient to activate vinculin. *J Biol Chem* 281:7228–7236.
43. Choi H-J, Huber AH, Weis WI (2006) Thermodynamics of β-catenin-ligand interactions: The roles of the N- and C-terminal tails in modulating binding affinity. *J Biol Chem* 281:1027–1038.